Journal of Alloys and Compounds 771 (2019) 607–613

Contents lists available at ScienceDirect

Journal of Alloys and Compounds

journal homepage: http://www.elsevier.com/locate/jalcom

# Phase transition in $BaThO_3$ from *Pbnm* to *Ibmm* turn the fundamental energy band gap from indirect to direct

A.H. Reshak [a, b, c], Z.A. Alahmed [b, *], J. Bila [a]

[a] Department of Instrumentation and Control Engineering, Faculty of Mechanical Engineering, CTU in Prague, Technicka 4, 166 07, Prague 6, Czech Republic
[b] Department of Physics and Astronomy, College of Science, P.O. Box 2455, King Saud University, Riyadh 11451, Saudi Arabia
[c] Nanotechnology and Catalysis Research Center (NANOCAT), University of Malaya, 50603, Kuala Lumpur, Malaysia

ARTICLE INFO

*Article history:*
Received 9 April 2018
Received in revised form
9 August 2018
Accepted 16 August 2018
Available online 30 August 2018

*Keywords:*
Phase transition
$BaThO_3$
*Pbnm*
*Ibmm*
DFT

ABSTRACT

The influence of phase transition on the electronic structure and the optical properties of $BaThO_3$ is investigated by means of density functional theory. At room temperature $BaThO_3$ is stable in the *Pbnm* phase, whereas it is stable in the *Ibmm* phase at high temperature. The transition from the *Pbnm* to the *Ibmm* phase cause a change in the band gap ($E_g$) nature from indirect to direct and a reduction by around 0.3 eV. The calculated $E_g$ is about 4.9 eV (*Pbnm*) and 4.6 eV (*Ibmm*). The phase transition influences the k-dispersion of bands around the Fermi level and, hence, the effective masses resulting in increasing the mobility of the charge carrier and enhancing the charge transfer mechanism. The obtained optical properties clearly show the influence of phase transition on the electronic structure. It was noticed that moving from *Pbnm* → *Ibmm* phase leads to shift the whole spectral structure towards lower energies by around 0.3 eV and increase the magnitudes of the optical components. It is found that the *Pbnm* and *Ibmm* phases exhibit negative uniaxial anisotropy and negative birefringence.



## 1. Introduction

In 1985, Kleykamp [1] observed the gray oxide phase with the perovskite type structure in the irradiated MOX (M = Ba, Sr and X = U, Pu, Zr, RE, Mo, and O=$O_3$) fuel. The probability of the formation of the multi-component oxides should be considered in the case of thoria-based fuels, too for example $BaThO_3$. Bharadwaj et al. [2] and Mishra et al. [3] measured Gibbs energy of $BaThO_3$ formation which indicates that barium thorate is likely to be formed within the thoria-based fuels from the component oxides. It has been reported that barium thorate $BaThO_3$ is very important member of the perovskite oxides family which display interesting physical properties [4–6]. At high temperature $ThO_2$ reacts with $BaCO_3$ to form $BaThO_3$ [7,8]. Nakamura [7] and Ohishi et al. [8] reported that $BaThO_3$ exists in cubic or orthorhombic phase. In 2013, Lebedev [9] theoretically predicted that $BaThO_3$ can be found in orthorhombic structure with two space groups i.e. *Pbnm* and *Ibmm* the later is the most stable phase which exists in room temperature. Heating $BaThO_3$ above 547 °C cause a phase transition to the *Ibmm* phase [7,10–14]. It has been reported that the two orthorhombic structures (*Pbnm* and *Ibmm*) show small energy difference and differ in the tilting of $ThO_6$ octahedra [9]. Several theoretical investigations on cubic $BaThO_3$ [7,9–16] and on orthorhombic phase and the possibility of the phase transition were reported [9].

Based on above and as natural extinction to our previous work on the cubic phase of $BaThO_3$ [16] we addressed ourselves to perform comprehensive theoretical investigation on the two phases (*Pbnm* and *Ibmm*) of orthorohombic-$BaThO_3$ using the density functional theory within the full-potential method. It is well known that the DFT approaches greatly improve the search efficiency and help experiments to save resources in the exploration of new crystals with good performance [17–30]. For instance, several researchers have used the DFT calculation for exploration the structure and optical properties of new material and found good agreement with the experimental results. We would like to mention here that, in our previous works [31–34], we have calculated the structure, energy band gap ($E_g$) and optical properties using full-potential method for several systems whose energy band gap and optical susceptibility dispersion are known experimentally and a very good agreement with the experimental data was obtained. Thus, we believe that our calculations reported in this paper would produce very accurate and reliable results.

* Corresponding author.
*E-mail address:* zalahmed@ksu.edu.sa (Z.A. Alahmed).

https://doi.org/10.1016/j.jallcom.2018.08.134
0925-8388/

## 2. Structural aspect and methodology

To investigate the ground state properties of orthorohombic-$BaThO_3$ in two phases (*Pbnm* and *Ibmm*), an *ab initio* first principle calculations are performed utilizing the full-potential method (wien2k code [35]) within the generalized gradient approximation (PBE-GGA) [36] to optimize the available lattice constant and the atomic positions [9]. The recently modified Becke-Johnson potential (mBJ) [37] is used to calculate the ground state properties from the relaxed structures of the two phases. The relaxed crystal structures of *Pbnm* and *Ibmm* phases are depicted in Fig. 1a and b.

The parameters that used in the *ab initio* calculations are; the basis functions in the interstitial region (IR) are expanded up to $R_{MT} \times K_{max} = 7.0$ and inside the atomic spheres for the wave function. The $\boldsymbol{l}_{max} = 10$ and the charge density is Fourier expanded up to $G_{max} = 12\ (\text{a.u.})^{-1}$. Self-consistency is obtained using 1000 $\vec{k}$ points in the irreducible Brillouin zone (IBZ). The self-consistent calculations are converged since the total energy of the system is stable within 0.00001 Ry. The electronic properties are calculated using 5000 $\vec{k}$ points in the IBZ. The input required for calculating the total and partial density of states (DOS) are the energy eigenvalues and eigenfunctions which are the natural outputs a band structure calculation. Therefore, from the band structure calculation the DOS are calculated by means of the modified tetrahedron method [38].

To reach accurate results, the muffin-tin spheres ($R_{MT}$) are chosen in such a way that the spheres did not overlap. Therefore, to ensure that no charge leakage is left out of the atomic sphere cores, the $R_{MT's}$ are chosen to be 2.49 atomic unit (a.u.) for Ba, 2.40 a.u. for Th and 1.96 a.u. for O in the *Pbnm* phase, while in the *Ibmm* phase the $R_{MT's}$ are chosen to be 2.5 a.u. (Ba), 2.41 a.u. (Th) and 1.97 a.u. (O).

## 3. Results and discussion

The calculated electronic band structure of *Pbnm* and *Ibmm* phases are shown in Fig. 2 a, b. It shows that moving from *Pbnm* to *Ibmm* cause to turn the $E_g$ of $BaThO_3$ from indirect to direct with a

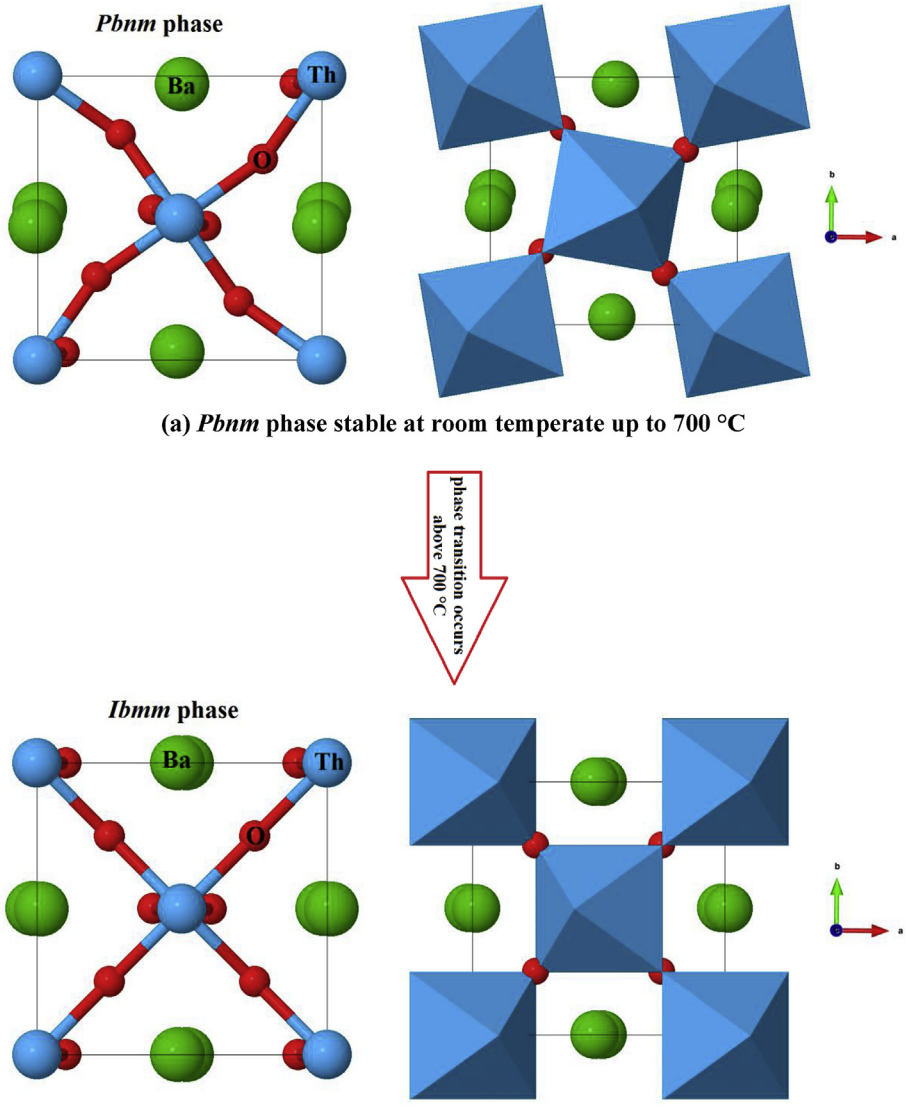


**Fig. 1.** (a, b) The crystal structure of *Pbnm* and *Ibmm* phases of $BaThO_3$.

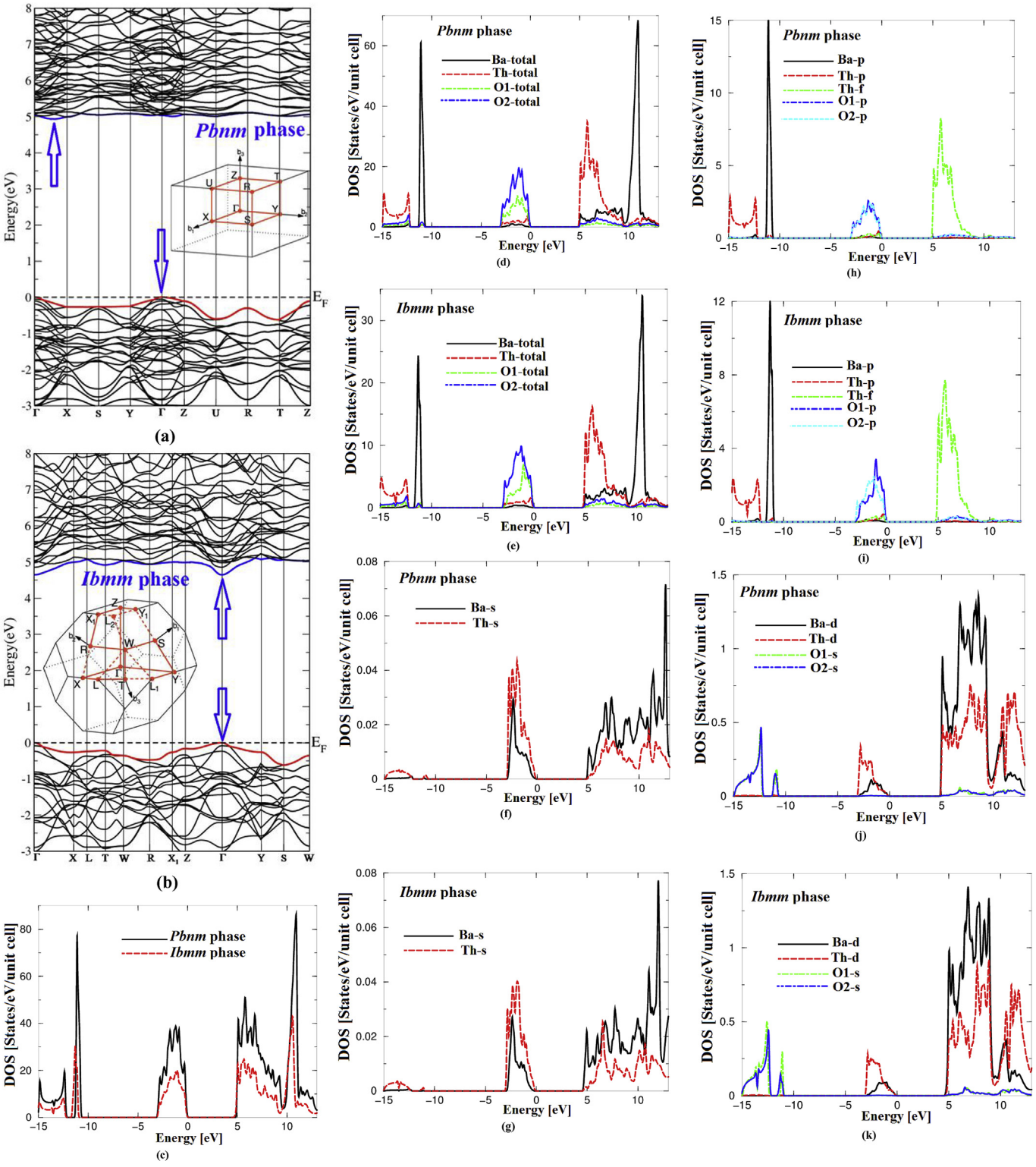


**Fig. 2.** (a, b) The calculated electronic band structure along with the first Brillouin zone of *Pbnm* and *Ibmm* phases of $BaThO_3$; **(c–k)** The calculated total and partial density of states of *Pbnm* and *Ibmm* phases of $BaThO_3$.

reduction by around 0.3 eV. Further, the first BZ of each phase is depicted along the electronic band structure which clearly show the high symmetry points of each phase, these symmetry points are given in Fig. 2a and b. From the electronic band structure (Fig. 2a and b) one can see that the high k-dispersion bands around Fermi level ($E_F$) possess low effect masses ($m_e^*$ and $m_h^*$) and, hence, the high mobility carriers (Table 1) which favor to enhance the charge transfer process. Both $m_e^*$ and $m_h^*$ provides essential information about the charge transfer mechanism. Moreover, the great effective mass difference ($D = m_e^*/m_h^*$) between electron ($e$) and hole ($h$)

**Table 1**
Calculated effective masses.

| Effective mass | *Pbnm* phase | *Ibmm* phase |
|---|---|---|
| $m_e^*/m_o$ | 0.03753 | 0.01203 |
| $m_{hh}^*/m_o$ | 0.03478 | 0.02765 |
| $m_{lh}^*/m_o$ | 0.01864 | 0.01871 |
| $D = m_{hh}^*/m_e^*$ | 0.92672 | 2.29842 |
| $D = m_e^*/m_{hh}^*$ | 1.07906 | 0.43508 |
| $D = m_{lh}^*/m_e^*$ | 0.49666 | 1.55527 |
| $D = m_e^*/m_{lh}^*$ | 2.01341 | 0.64297 |

(Table 1) can facilitate the *e* and *h* migration and separation, and finally improve the charge transfer performance. The large mobility difference is useful to the separation of *e* and *h*, reduction of *e* and *h* recombination rate, and improvement of the charge transfer activity. It is clear that from Table 1, the $m_e^*/m_o$ in *Pbnm* phase is bigger than that of the heavy and light holes while the *Ibmm* phase possess $m_e^*/m_o$ lower than both of heavy and light holes, resulting in a significant difference in the mobility between *e* and *h*. However, one can deduce that the carrier transfer can be fast along different directions.

The total density of states for *Pbnm* and *Ibmm* phases explore the influence of the phase transition on the band dispersion and the $E_g$ reduction (Fig. 2c). Deep insight into the electronic structure can be gained from the calculated partial density of states (PDOS) of each orbital. Fig. 2 d–k illustrates the contribution of each atom and their orbitals to the band structure of each phase. It is clear that the phase transition causes significant influence to the dispersion of each orbital. Also, it causes to influence the hybridizations between the orbitals for instance in *Pbnm* phase the O1-p orbital strongly hybridized with O2-p orbital, this hybridization disappears in the *Ibmm* phase. Further, in *Pbnm* phase the O1-s orbital strongly hybridized with O2-s orbital, while the transition to *Ibmm* phase cause to weaken this hybridization. It is interested to highlight that the hybridization may lead to form covalent bonding depending on the degree of the hybridization, which is more favorable for the transport of the carriers than ionic one [39]. We make use of the calculated PDOS to elucidate the chemical bonding characters for the two phases. In the valence bands between −12.0 eV and $E_F$, we have obtained a total number of electrons/eV (*e*/*eV*) for the orbitals in each atom for *Pbnm* (*Ibmm*) phase of $BaThO_3$ as follow: Ba-p orbital 15 (12) *e*/*eV*, O1-p orbital 3 (3.9) *e*/*eV*, O2-p orbital 3 (3.7) *e*/*eV*, Ba-s orbital 0.03 (0.029) *e*/*eV*, Th-s orbital 0.o45 (0.042) *e*/*eV*, O1-s orbital 0.15 (0.13) *e*/*eV*, O2-s orbital 0.2 (0.3) *e*/*eV*, Ba-d orbital 0.125 (0.12) *e*/*eV* and Th-d orbital 0.35 (0.3) *e*/*eV*. Thus, following the obtained total number of electrons/eV one can conclude that some electrons from Ba, Th and O atoms are transferred into valence bands and contribute in covalence interactions between the atoms, according to the contribution of each atom to the valence bands. The strength/weakness of the covalence interactions arises due to the degree of the hybridization and the electronegativity differences between the atoms. Thus, the PDOS help us to analyze the nature of the bonds following the classical chemical concept. This concept is very useful to classify compounds into different categories with respect to different chemical and physical properties. To support this observation, the valence charge density distributions of the two phases are calculated and presented in (1 0 0) and (1 0 1) crystallographic planes as shown in Fig. 3 a–d. These crystallographic planes clearly show the influence of the phase transition on the charge distribution around each atom. For instance, in the area marked by "A" in (1 0 0) crystallographic plane of the two phases which is surrounded by four oxygen atoms, the transitions *Pbnm* →*Ibmm* cause to push O1 and O4 atoms towards "A" resulting in significant perturbation to the contours which surrounding the area "A". More detailed information about the influence of the phase transition can be obtained from (1 0 1) crystallographic planes (Fig. 3 c,d). These plots clearly show that the phase transition cause very significant influence in the (1 0 1) plane in the matter of the atom sites and the charge distribution. Using the map of electronic charge density distribution, one can analyze the nature of bonding among the atoms in *Pbnm* and *Ibmm* phases of $BaThO_3$. The transfer of charge between the anion and cation can be utilized to explain the ionic characters whereas sharing the charge between anion and cation is related to the covalent character. Based on this one can explain the influence of the phase transition on the bonding nature in the two phases. The bond between Th and O is mostly ionic and partially covalent and the same for Ba-O bond. According to Pauling scale, the electro-negativity of Ba, Th and O are 0.89 < 1.3< 3.44. For the description of the bonding character, the difference of the electro-negativity ($X_A$-$X_B$) is crucial [40], where $X_A$ and $X_B$ are the electro-negativity of the A and B atoms. The percentage of the ionic character P(%) of the bonding can be obtained follow the expression [40]:

$$P(\%) = 16(X_A - X_B) + 3.5(X_A - X_B)^2 \quad (1)$$

Following this expression, one can obtained the P(%) of Ba-O to be 63.55 and Th-O is about 50.26 indicated that a charge transfer occurs towards O atoms, as it is shown by the blue uniform spheres surrounded O atoms indicating the maximum charge accumulated according to the thermo-scale (Fig. 4e) [41]. It has been reported by Ohishi et al. [8] that the weak Ba-O bonds could be the reason for the larger thermal expansion of $BaThO_3$ which is much more than $ThO_2$, and hence, low thermal conductivity therefore, the precipitation of $BaThO_3$ will significantly reduce the thermal conductivity of the oxide fuel.

Deep insight into the electronic structure can be obtained from the calculated optical properties for the two phases of $BaThO_3$. The obtained optical properties clearly show the influence of the phase transition on the electronic structure. Fig. 4 a,b illustrated $\varepsilon_2(\omega)$ and $\varepsilon_1(\omega)$. These figures reveal the different spectral structure for *Pbnm* and *Ibmm* phases, and, hence the electronic structure of the two phases, since the optical transitions originates from inter-band transitions between valence and conduction band states according to the dipole selection rule. The later state that, only transitions changing the angular momentum quantum number *l* by unity are allowed. It was noticed that moving from *Pbnm* phase to *Ibmm* phase lead to shift whole spectral structure towards lower energies by around 0.3 eV and increase the magnitudes of the optical components. It is clearly seen that the dispersion of the optical spectra of *Pbnm* phase (Fig. 4a) differ than that of *Ibmm* phase (Fig. 4b) indicating that this differ as a consequence of the phase transition. From $\varepsilon_1(\omega)$ one can gain very valuable information for instance the vanishing frequency value in the dielectric function which defines the static electronic dielectric constant by $\varepsilon_\infty = \varepsilon_1(0)$. It is clear that $\varepsilon_1(0)$ for the *Pbnm* phase is smaller than that of *Ibmm* phase (Table 2). Furthermore, $\varepsilon_\infty = \varepsilon_1(0)$ is inversely related to $E_g$ this can be explained on the basis of the Penn model [42]. One of the important features of the optical spectra is the plasmon oscillations $\omega_p^{xx}$, $\omega_p^{yy}$ and $\omega_p^{zz}$. The plasmon oscillations are associated with inter-band transitions that occur at energies where optical spectra of $\varepsilon_1^{xx}(\omega)$, $\varepsilon_1^{yy}(\omega)$, $\varepsilon_1^{zz}(\omega)$ cross zero. The values of $\omega_p^{xx}$, $\omega_p^{yy}$ and $\omega_p^{zz}$ for *Pbnm* phase are much differ than that of *Ibmm* phase as shown in Table 2. The other important feature is the uniaxial anisotropy ($\delta\varepsilon$) [31], which can be calculated from $\varepsilon_1^{xx}(0)$, $\varepsilon_1^{yy}(0)$, $\varepsilon_1^{zz}(0)$. It is found that *Pbnm* and *Ibmm* phases exhibit negative $\delta\varepsilon$, as shown in

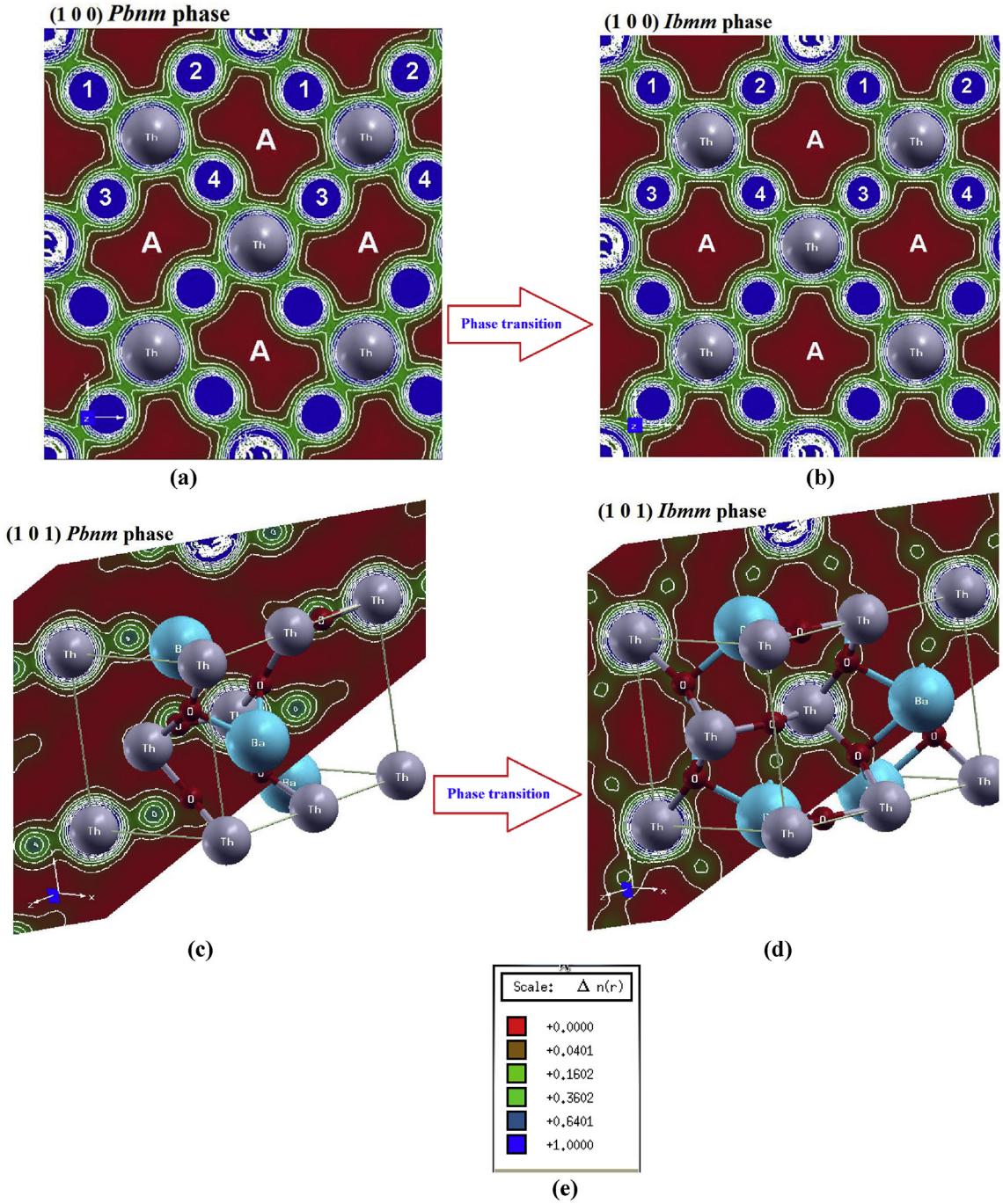


**Fig. 3.** Calculated electronic charge density distribution of *Pbnm* and *Ibmm* phases of $BaThO_3$; **(a, b)** crystallographic plane (1 0 0); **(c, b)** crystallographic plane (1 0 1); **(e)** thermo-scale.

Table 2. The optical conductivity (Fig. 4 c, d) which consists of imaginary and real parts and completely characterizes the linear optical properties confirm the influence of the phase transition on the optical response.

The optical reflectivity spectra of *Pbnm* (*Ibmm*) phases (Fig. 4e, f) show that at low energies the two phases exhibit low reflectivity. The first reflectivity maxima occurs at around 10.0 (11.0) eV, followed by the first reflectivity minima which is situated at around 11.5 (11.0) eV, confirming the occurrence of a collective plasmon resonance in concordance with our observation in Fig. 4 a, b. Fig. 4 g, h show the loss function of the two phases of $BaThO_3$. The region confined between 11.0 and 12.0 eV represents the lossless region. The loss function's peaks are initiated at the values of the plasma frequencies $\omega_p^{xx}$ , $\omega_p^{yy}$ and $\omega_p^{zz}$. These peaks represent the negative part of $\varepsilon_1^{xx}(\omega)$, $\varepsilon_1^{yy}(\omega)$, $\varepsilon_1^{zz}(\omega)$. The absorption coefficient (Fig. 4i and j) can be divided into four regions, the low absorption region, high absorption region, lossless region and high transparent region. The absorption edges of the three tensor components occur at 4.9 (4.6) eV. Further, we have calculated the refractive indices from the complex dielectric function, as shown in Fig. 4 k, l. The calculated values of $n^{xx}(0)$, $n^{yy}(0)$, $n^{zz}(0)$ and $\Delta n(\omega)$ are shown in Table 2. It is clear that both phases exhibit negative birefringence. The

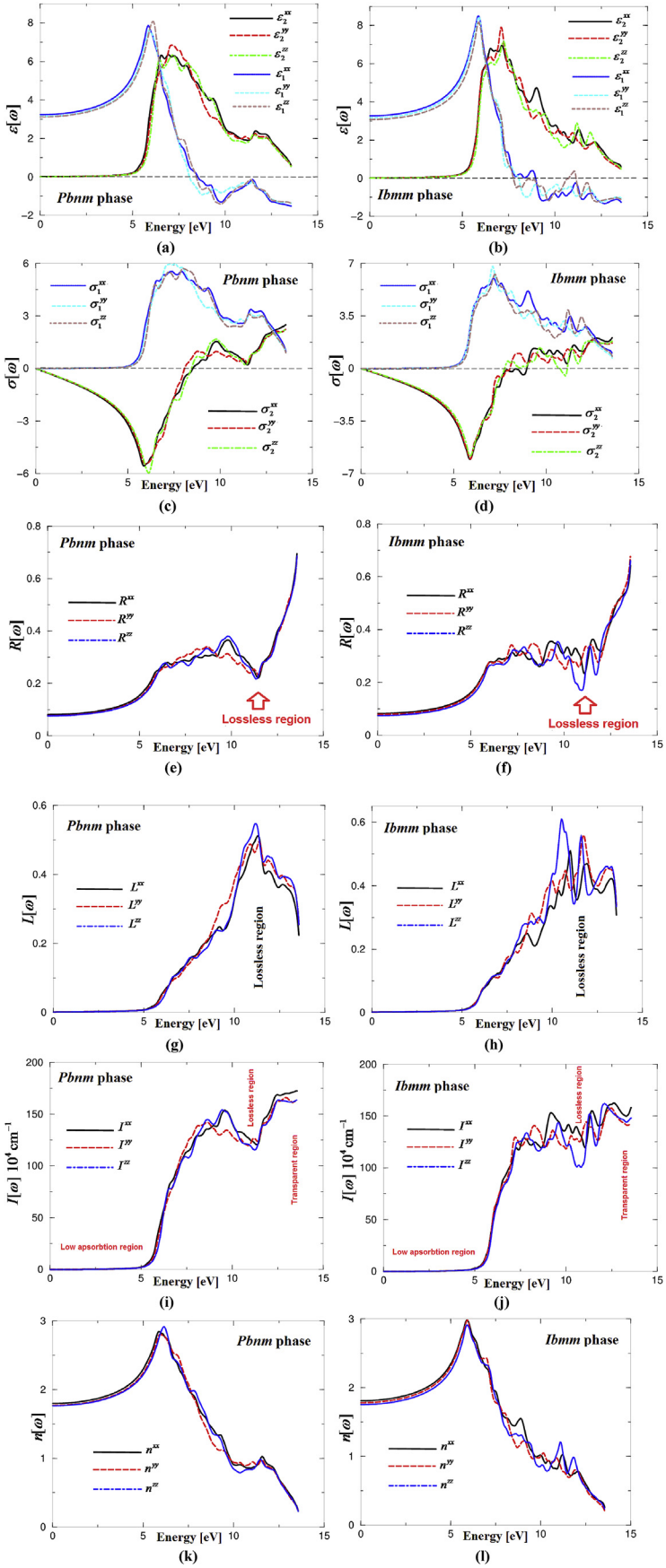


**Fig. 4.** (a, b) Calculated $\varepsilon_2^{xx}(\omega)$ (dark solid curve-black color online), $\varepsilon_2^{yy}(\omega)$ (light long dashed curve-red color online) and $\varepsilon_2^{zz}(\omega)$ (light dotted dashed curve -green color online) along with Calculated $\varepsilon_1^{xx}(\omega)$ (dark solid curve-blue color online), $\varepsilon_1^{yy}(\omega)$ (light dashed curve-brown color online) and $\varepsilon_1^{zz}(\omega)$ (light sold curve -violet color online) of *Pbnm* and *Ibmm* phases of $BaThO_3$; (c, d) Calculated $\sigma_2^{xx}(\omega)$ (dark solid curve-black color online), $\sigma_2^{yy}(\omega)$ (light dashed curve-red color online) and $\sigma_2^{zz}(\omega)$ (light dotted dashed curve -green color online) along with Calculated $\sigma_1^{xx}(\omega)$ (dark solid curve-blue color online), $\sigma_1^{yy}(\omega)$ (light dashed curve-red brown online) and $\sigma_1^{zz}(\omega)$ (light solid curve - violet color online) of *Pbnm* and *Ibmm* phases of $BaThO_3$**; (e, f)** Calculated $R^{xx}(\omega)$ (dark solid curve-black color online), $R^{yy}(\omega)$ (light dashed curve-red color online), and $R^{zz}(\omega)$ (light dotted dashed curve -blue color online) of *Pbnm* and *Ibmm* phases of $BaThO_3$; **(g, h)** Calculated loss function $L^{xx}(\omega)$ (dark solid curve-back color online), $L^{yy}(\omega)$ (light dashed curve-red color online) and $L^{zz}(\omega)$ (light dotted dashed curve -blue color online) spectrum of *Pbnm* and *Ibmm* phases of $BaThO_3$; **(i, j)** Calculated loss function $\sigma_1^{xx}(\omega)$ (dark solid curve-back color online), $\sigma_1^{yy}(\omega)$ (light dashed curve-red color online) and $\sigma_1^{zz}(\omega)$ (light dotted dashed curve -blue color online) spectrum of *Pbnm* and *Ibmm* phases of $BaThO_3$; **(c)** Calculated refractive indices $n^{xx}(\omega)$ (dark solid curve-black color online), $n^{yy}(\omega)$ (light dashed curve-red color online) and $n^{zz}(\omega)$ (light dotted dashed curve -blue color online) spectrum of *Pbnm* and *Ibmm* phases of $BaThO_3$.

**Table 2**
The calculated $\varepsilon_1^{xx}(0)$, $\varepsilon_1^{yy}(0)$, $\varepsilon_1^{zz}(0)$, $\delta\varepsilon$, $\omega_p^{xx}$, $\omega_p^{yy}$, $\omega_p^{zz}$, $n^{xx}(0)$, $n^{yy}(0)$, $n^{zz}(0)$ and $\Delta n(0)$.

| Component | *Pbnm* phase | *Ibmm* phase |
|---|---|---|
| $\varepsilon_1^{xx}(0)$ | 3.234 | 3.273 |
| $\varepsilon_1^{yy}(0)$ | 3.137 | 3.173 |
| $\varepsilon_1^{zz}(0)$ | 3.116 | 3.079 |
| $\delta\varepsilon$ | −0.033 | −0.046 |
| $\omega_p^{xx}$ | 8.530 | 8.966 |
| $\omega_p^{yy}$ | 8.095 | 8.068 |
| $\omega_p^{zz}$ | 8.449 | 7.768 |
| $n^{xx}(0)$ | 1.798 | 1.809 |
| $n^{yy}(0)$ | 1.771 | 1.781 |
| $\Delta n(0)$ | 1.765 | 1.754 |
| $\Delta n(0)$ | −0.030 | −0.041 |

calculated optical properties show a considerable anisotropy in the energy region between 7.0 eV and 12.0 eV.

## 4. Conclusion

Using the full potential method within mBJ the influence of phase transition on the electronic structure and the optical properties of $BaThO_3$ is comprehensively investigated. It was found that transition from *Pbnm* to *Ibmm* phase cause to change the band gap nature from indirect to direct and band gap reduction from 4.9 eV to 4.6 eV. The phase transition influences the k-dispersion of bands around Fermi level and, hence, the effective masses resulting in increasing the mobility of the charge carrier and enhancing the charge transfer mechanism. The obtained optical properties clearly show that moving from *Pbnm* phase to *Ibmm* phase leads to shift the whole spectral structure towards lower energies by around 0.3 eV and increase the magnitudes of the optical components. It was found that the phase transition cause to increase the negativity of the uniaxial anisotropy and birefringence values.

## Acknowledgments

The authors (A.H.R and Z.A.A) extend their appreciation to the International Scientific Partnership Program ISPP at King Saud University for funding this research work through ISPP# 0016.

## References

[1] H. Kleykamp, J. Nucl. Mater. 131 (1985) 221–246.
[2] S.R. Bharadwaj, R. Mishra, M. Ali, D. Das, A.S. Kerkar, S.R. Dharwadkar, J. Nucl. Mater. 275 (1999) 201–205.
[3] R. Mishra, M. Ali, S.R. Bharadwaj, A.S. Kerkar, D. Das, S.R. Dharwadkar, J. Alloys Compd. 290 (1999) 97–102.
[4] H.P.R. S.H. Noble, Activated electrode, U.S. Patent No. 2,394,095, 05 February, 1946.
[5] J.E. White, Thermoionic electrode for discharge lamps, U.S. Patent No. 3,029,359, 10 April, 1962.
[6] D.M. Speros, Cathodes and method of manufacture, U.S. Patent No. 3,188,236, 08 June, 1965.
[7] T. Nakamura, Chem. Lett. (1974) 429–434, https://doi.org/10.1246/cl.1974.429.
[8] Y. Ohishi, E. Yusnitha, K. Kurosaki, H. Muta, S. Yamanaka, J. Nucl. Mater. 448 (2014) 62–65.
[9] A.I. Lebedev, J. Alloys Compd. 580 (2013) 487–490.
[10] R.V. Krishnan, K. Nagarajan, P.R.V. Rao, J. Nucl. Mater. 299 (2001) 28–31.
[11] G. Murphy, B.J. Kennedy, B. Johannessen, J.A. Kimpton, M. Avdeev, C.S. Griffith, G.J. Thorogood, Z.M. Zhang, J. Solid State Chem. 237 (2016) 86–92.
[12] D.J. Gregg, Z.M. Zhang, G.J. Thorogood, B.J. Kennedy, J.A. Kimpton, G.J. Griffiths, P.R. Guagliardo, G.R. Lumpkin, E.R. Vance, J. Nucl. Mater. 452 (2014) 474–478.
[13] G.L. Murphy, B.J. Kennedy, J.A. Kimpton, Q.F. Gu, B. Johannessen, G. Beridze, P.M. Kowalski, D. Bosbach, M. Avdeev, Z.M. Zhang, Inorg. Chem. 55 (2016) 9329–9334.
[14] E. Reynolds, B.J. Kennedy, M. Avdeev, G.J. Thorogood, Z.M. Zhang, H.E.A. Brand, J. Solid State Chem. 243 (2016) 8–11.
[15] G. Murtaza, I. Ahmad, B. Amin, A. Afaq, M. Maqbool, J. Maqssod, I. Khan, M. Zahid, Opt. Mater. 33 (2011) 553–557.
[16] Z. Ali, I. Ahmad, A.H. Reshak, Physica B 410 (2013) 217–221.
[17] Z.S. Lin, X.X. Jiang, L. Kang, P.F. Gong, S.Y. Luo, M.H. Lee, J. Phys. D Appl. Phys. 47 (2014), 253001.
[18] M.I. Kolinko, I.V. Kityk, A.S. Krochuk, J. Phys. Chem. Solids 53 (1992) 1315–1320.
[19] G.E. Davydyuk, O.Y. Khyzhun, A.H. Reshak, H. Kamarudin, G.L. Myronchuk, S.P. Danylchuk, A.O. Fedorchuk, L.V. Piskach, M.Y. Mozolyuk, O.V. Parasyuk, Phys. Chem. Chem. Phys. 15 (2013) 6965–6972.
[20] A.H. Reshak, Y.M. Kogut, A.O. Fedorchuk, O.V. Zamuruyeva, G.L. Myronchuk, O.V. Parasyuk, H. Kamarudin, S. Auluck, K.J. Plucinski, J. Bila, Phys. Chem. Chem. Phys. 15 (2013) 18979–18986.
[21] V.V. Atuchin, T.A. Gavrilova, J.C. Grivel, V.G. Kesler, Surf. Sci. 602 (2008) 3095–3099.
[22] V.V. Atuchin, T.A. Gavrilova, J.C. Grivel, V.G. Kesler, J. Phys. D Appl. Phys. 42 (2009), 035305.
[23] O.Y. Khyzhun, V.L. Bekenev, V.V. Atuchin, E.N. Galashov, V.N. Shlegel, Mater. Chem. Phys. 140 (2013) 588–595.
[24] V.V. Atuchin, E.N. Galashov, O.Y. Khyzhun, V.L. Bekenev, L.D. Pokrovsky, Y.A. Borovlev, V.N. Zhdankov, J. Solid State Chem. 236 (2016) 24–31.
[25] H.W. Huang, X. Han, X.W. Li, S.C. Wang, P.K. Chu, Y.H. Zhang, ACS Appl. Mater. Interfaces 7 (2015) 482–492.
[26] H.W. Huang, X.W. Li, J.J. Wang, F. Dong, P.K. Chu, T.R. Zhang, Y.H. Zhang, ACS Catal. 5 (2015) 4094–4103.
[27] Angew. Chem. Int. Ed. 45 (2006) 2100–2103.
[28] I.V. Kityk, P. Bragiel, M. Piasecki, B. Sahraoui, P. Hudhomme, A. Gorgues, Phase Transit. 74 (2001) 347–352.
[29] W.H. Bi, N. Louvain, N. Mercier, J. Luc, I. Rau, F. Kajzar, B. Sahraoui, Adv. Mater. 20 (2008) 1013–1017.
[30] B. Sahraoui, R. Czaplicki, A. Klöpperpieper, A.S. Andrushchak, A.V. Kityk, J. Appl. Phys. 107 (2010), 113526.
[31] A.H. Reshak, Sci. Rep. 7 (2017), https://doi.org/10.1038/srep46415, 46415.
[32] A.H. Reshak, S. Auluck, RSC Adv. 7 (2017) 14752–14760.
[33] A.H. Reshak, M.G. Brik, J. Alloys Compd. 675 (2016) 355–363.
[34] A.H. Reshak, J. Appl. Phys. 119 (2016), 105706.
[35] P. Blaha, K. Schwarz, G. Madsen, D. Kvasnicka, J. Luitz, wien2k, An Augmented Plane Wave+ Local Orbitals Program for Calculating Crystal Properties, 2001.
[36] J.P. Perdew, K. Burke, M. Ernzerhof, Phys. Rev. Lett. 77 (1996) 3865–3868.
[37] F. Tran, P. Blaha, Phys. Rev. Lett. 102 (2009), 226401.
[38] P.E. Blochl, O. Jepsen, O.K. Andersen, Phys. Rev. B 49 (1994) 16223–16233.
[39] F. Wu, H.Z. Song, J.F. Jia, X. Hu, Prog. Nat. Sci. Mater. 23 (2013) 408–412.
[40] Schlusseltechnologien Key Technologies, 41st IFF Springschool, 2010, pp. A1–A18.
[41] C.Y. Liu, Y.H. Zhang, F. Dong, A.H. Reshak, L.Q. Ye, N. Pinna, C. Zeng, T.R. Zhang, H.W. Huang, Appl. Catal. B Environ. 203 (2017) 465–474.
[42] D.R. Penn, Phys. Rev. 128 (1962) 2093.